

$J_{\text{eff}} = 3/2$ metallic phase and unconventional superconductivity in GaTa₄Se₈

Min Yong Jeong,¹ Seo Hyoung Chang,² Hyeong Jun Lee,³ Jae-Hoon Sim ^{1,4} Kyeong Jun Lee,² Etienne Janod,⁵ Laurent Cario,⁵ Ayman Said,⁶ Wenli Bi ⁷ Philipp Werner,⁸ Ara Go ^{3,9,*} Jungho Kim,^{6,†} and Myung Joon Han ^{1,‡}

¹Department of Physics, Korea Advanced Institute of Science and Technology, Daejeon 34141, Korea

²Department of Physics, Chung-Ang University, Seoul 06974, South Korea

³Center for Theoretical Physics of Complex Systems, Institute for Basic Science (IBS), Daejeon 34126, Korea

⁴CPHT, CNRS, Ecole Polytechnique, Institut Polytechnique de Paris, F-91128 Palaiseau, France

⁵Institut des Matériaux Jean Rouxel (IMN), Université de Nantes, CNRS, 2 Rue de la Houssinière, BP32229, 44322 Nantes Cedex 3, France

⁶Advanced Photon Source, Argonne National Laboratory, Argonne, Illinois 60439, USA

⁷Department of Physics, University of Alabama at Birmingham, Birmingham, Alabama 35294, USA

⁸Department of Physics, University of Fribourg, 1700 Fribourg, Switzerland

⁹Department of Physics, Chonnam National University, Gwangju 61186, Korea

 (Received 22 June 2020; revised 16 September 2020; accepted 5 February 2021; published 24 February 2021)

By means of density functional theory plus dynamical mean-field theory (DFT + DMFT) calculations and resonant inelastic x-ray scattering (RIXS) experiments, we investigate the high-pressure phases of the spin-orbit-coupled $J_{\text{eff}} = 3/2$ insulator GaTa₄Se₈. Its metallic phase, derived from the Mott state by applying pressure, is found to carry $J_{\text{eff}} = 3/2$ moments. The characteristic excitation peak in the RIXS spectrum maintains its destructive quantum interference of J_{eff} at the Ta L_2 edge up to 10.4 GPa. Our exact diagonalization-based DFT + DMFT calculations including spin-orbit coupling also reveal that the $J_{\text{eff}} = 3/2$ character can be clearly identified under high pressure. These results establish the intriguing nature of the correlated metallic magnetic phase, which represents the first confirmed example of $J_{\text{eff}} = 3/2$ moments residing in a metal. They also indicate that the pressure-induced superconductivity is likely unconventional and influenced by these $J_{\text{eff}} = 3/2$ moments. Based on a self-energy analysis, we furthermore propose the possibility of doping-induced superconductivity related to a spin-freezing crossover.

DOI: [10.1103/PhysRevB.103.L081112](https://doi.org/10.1103/PhysRevB.103.L081112)

Introduction. Identifying and characterizing the phases and phase transitions of materials is a central theme of condensed-matter physics. The discovery of a new type of phase often requires theoretical analyses of its essential nature, as well as clarifications of the relationship to other known phases and the possible transitions into nearby phases. As a well-known example, unconventional metal states in cuprate phase diagrams hold many mysteries [1–4]. Being clearly different from a Fermi liquid, these anomalous metallic phases can be a precursor or a competitor of unconventional superconductivity [5–7].

The lacunar spinels GaM₄X₈ ($M = \text{V, Nb, Ta, Mo}$; $X = \text{S, Se, Te}$) are a fascinating class of materials which exhibit multiferroic, skyrmion, and resistive switching phenomena [8–14]. GaTa₄Se₈, in particular, has been highlighted as an interesting example that undergoes a paramagnetic Mott insulator to metal transition (IMT) under pressure [15–18]. Furthermore, recent studies have elucidated the significant effect of spin-orbit coupling (SOC) and have shown that its ground state carries spin-orbit-entangled (so-called) $J_{\text{eff}} = 3/2$ moments [19–21], which is the first confirmed example of this

kind. Considering the observed IMT followed by a superconducting transition as a function of pressure, the identification of the $J_{\text{eff}} = 3/2$ Mott phase under ambient conditions immediately generates a series of important questions: If the metallic phase is a conventional Fermi liquid, it is a more or less trivial case, and the superconductivity observed at higher pressures is also likely of the conventional type. On the other hand, if it is a correlated metal which still hosts $J_{\text{eff}} = 3/2$ moments, it can be regarded as a new type of metallic phase, and the observed superconductivity is more likely to be unconventional.

In this Letter, we try to elucidate the nature of the pressure-induced metallic phase which emerges out of the Mott insulator without doping. By means of resonant inelastic x-ray scattering (RIXS) experiments and density functional theory plus dynamical mean-field theory (DFT + DMFT) calculations, we investigate its detailed electronic and magnetic properties. We find that the characteristic L_3 peak is clearly observed even in the metallic regime while the forbidden L_2 peak is absent. This observation together with the simulation results clearly identifies a distinct metallic state with $J_{\text{eff}} = 3/2$ magnetic moments. We discuss its implications regarding the superconductivity at higher pressure. Finally, we explore another intriguing possibility in this material. Our self-energy analysis shows that electron doping can induce a spin-freezing crossover, a phenomenon which has been previously linked

* arago@jnu.ac.kr

† jhkim@anl.gov

‡ mj.han@kaist.ac.kr

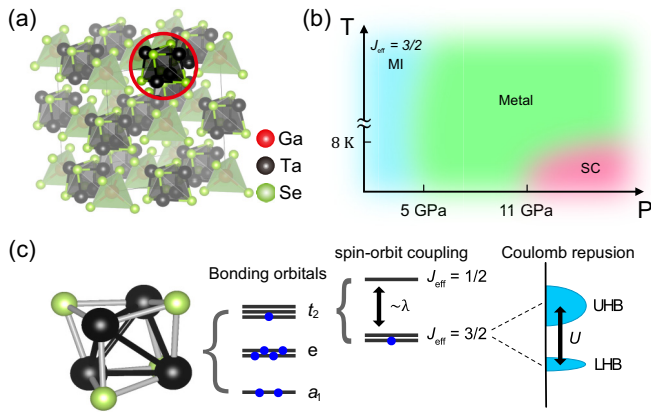


FIG. 1. (a) Crystal structure of GaTa_4Se_8 . Red, black, and green spheres represent the Ga, Ta, and Se atoms, respectively. (b) A schematic pressure-temperature phase diagram of GaTa_4Se_8 . The cyan, green, and red colored regions represent the $J_{\text{eff}} = 3/2$ Mott-insulating, metallic, and superconducting phases, respectively. It should be noted that the phase boundary lines have not yet been well identified due to the lack of experimental information. (c) Schematic electronic structure near E_F which is dominated by molecular orbital states of the higher-lying t_2 type and the lower-lying e and a_1 types. The t_2 levels are further split into $J_{\text{eff}} = 1/2$ and $3/2$ by SOC. At ambient pressure, the Mott gap is stabilized by the on-site Coulomb interaction U .

to unconventional superconductivity [22]. These results will hopefully stimulate experimental efforts to clarify the properties of this material under chemical or other types of doping.

Electronic structure and insulator-metal-superconductor transition. GaTa_4Se_8 is composed of well-separated GaSe_4 and Ta_4Se_4 molecular clusters as shown in Fig. 1(a). The Fermi level (E_F) is dominated by t_2 molecular orbitals which are derived from Ta t_{2g} atomic orbitals [14–18,20,21,23,24]. On top of the spin-orbit split molecular $J_{\text{eff}} = 3/2$ quartet and the $J_{\text{eff}} = 1/2$ doublet, the on-site Coulomb interaction (U) induces a Mott gap in the quarter-filled $J_{\text{eff}} = 3/2$ bands (see Fig. 1(c) [20,21]). This spin-orbit-entangled molecular $J_{\text{eff}} = 3/2$ Mott phase was first predicted by DFT + SOC + U calculations [20] and then confirmed by RIXS experiments [21]. Here the “on-site” Coulomb repulsion U represents the interaction within molecular t_2 orbitals rather than atomic Ta orbitals [16,18,23].

Largely unexplored are the IMT and the metal-to-superconductor transition, both of which are induced by applying pressure [without doping; see Fig. 1(b)] [15–18]. The pressure-dependent crystal structure data [16] indicate that the Mott IMT is caused by the increased hopping integrals between the Ta_4Se_4 molecular units. This bandwidth-controlled IMT was studied based on the three-orbital Hubbard model within DMFT-QMC (quantum Monte Carlo) [18]. However, the effect of SOC was not taken into account and therefore the $J_{\text{eff}} = 3/2$ state could not be realized.

DFT + DMFT phase diagram: The effect of SOC. With this motivation, we first performed DFT + DMFT calculations with SOC (see Supplemental Material for computation details [25]). The calculated phase diagram is presented in Fig. 2. The red and blue colored regions represent the insulating and

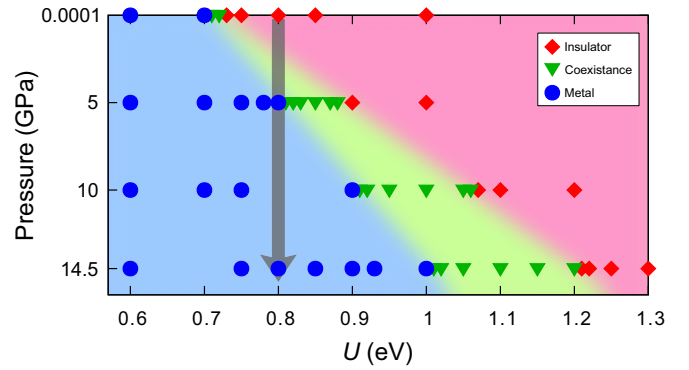


FIG. 2. Calculated phase diagram for GaTa_4Se_8 as a function of U and pressure within DFT + DMFT + SOC (at zero temperature). Blue circles, red diamonds, and green triangles represent the calculated points corresponding to the metallic, insulating, and coexistence phases, respectively. The realistic value of $U \approx 0.8$ eV is depicted by a gray arrow.

metallic phases, respectively. We note that at $U > 0.7$ eV the pressure can always induce the transition and that the critical value of U_c is gradually increased as the pressure increases.

By including SOC, the calculated phase diagram shows a good quantitative agreement with the experiments. Considering the neglected frequency dependence of U in the DMFT procedure, we expect that the realistic effective interaction strength is slightly larger than the constrained random phase approximation (cRPA) value of $U_{\text{cRPA}} = 0.7$ eV; $U \approx 0.7$ – 0.9 eV [26]. With $U = 0.8$ eV, the IMT occurs at $P \approx 5$ GPa as shown in Fig. 2. This is in good agreement with previous experimental data reporting a critical pressure P_c of 5–7 GPa [17,18]. It is important to note that, in the previous DMFT calculations (without SOC), the critical U_c of 1.2 eV [18] is significantly larger than our value. Also, if we follow Ref. [18] and identify the calculated coexistence region with the hysteresis region observed at intermediate pressure in the resistivity measurement [18], our results are in even better agreement with the experiment. Hence, without the effect of SOC, the experimental phase boundary cannot be well reproduced and the $J_{\text{eff}} = 3/2$ moments are not formed.

Metallic $J_{\text{eff}} = 3/2$ states: RIXS experiment. The direct evidence of the $J_{\text{eff}} = 3/2$ Mott phase at ambient pressure came from RIXS [21]. As an element-specific photon-in and photon-out measurement using dipole transitions between Ta $5d$ and $2p_{3/2}$ (L_3) or $2p_{1/2}$ (L_2), RIXS was able to detect and compare the excitation spectra at both edges. The compelling evidence for $J_{\text{eff}} = 3/2$ was the presence and the absence of an ~ 1.3 -eV peak at L_3 and L_2 , respectively, which is directly based on the quantum mechanical selection rules [21]. Here we adopt the same approach to probe $J_{\text{eff}} = 3/2$ moments in the metallic regime and perform pressure-dependent RIXS measurements (see Supplemental Material for experimental details [25]).

Figure 3(a) shows the RIXS spectra at the L_3 edge under pressure. The positive sign in the energy represents energy loss. Strong low-energy intensities for all high pressures are mostly attributed to an extrinsic scattering from high-pressure environments such as the Be gasket and the diamond anvils,

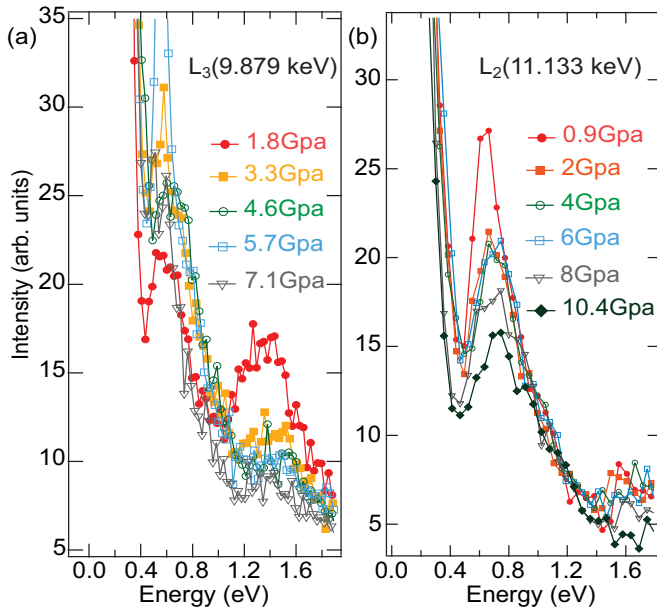


FIG. 3. [(a),(b)] Pressure-dependent RIXS data at the (a) L_3 and (b) L_2 edges. The different symbols and colors represent different pressure values.

and those intensity tails largely affect the spectral features below 0.4 eV [27]. The insulating phase (1.8 GPa) spectrum shows two broad features around 0.7 and 1.3 eV. At higher pressures, low-energy high-pressure environment scattering intensities become stronger, leading to seemingly larger intensities around 0.7 eV, because the gasket and the diamond anvil become closer to the sample at high pressure. The sharp peak around 0.7 eV seen at 3.3 and 5.7 GPa comes from high-pressure environments. On the other hand, the 1.3-eV peak feature is marginally affected by the tail of the extrinsic scattering and free from any sharp high-pressure environment scattering peak. The 1.3-eV peak originates from the orbital excitation in between the occupied e and a_1 states and the unoccupied $J_{\text{eff}} = 1/2$ state [21]. The ambient pressure RIXS measurement showed that the 1.3-eV peak intensity is largely modulated with the crystal momentum transfer and the sample angle [21]. The 1.3-eV peak intensity is weak in the sample orientation used for the spectra in Fig. 3(a). It is important to note that the 1.3-eV broad feature is, although weak, visible up to the metallic phase (5.7 and 7.1 GPa) and its energy position and width more or less stay the same. For further analysis, see Supplemental Material [25].

Figure 3(b) presents our main experimental RIXS spectra at the L_2 edge under high pressure. In this high-pressure sample, the extrinsic scatterings from high-pressure environments happen to be weaker compared to the case of the L_3 -edge measurement, and therefore, we resolve orbital excitations above 0.4 eV without high-pressure environment contamination: the low-energy extrinsic scattering intensities are similar for all high pressures and no sharp high-pressure environment scattering peak is seen. The 0.7-eV peak at the L_2 edge was assigned, in the previous work, to excitations from the occupied e and a_1 states to the unoccupied $J_{\text{eff}} = 3/2$ states [21]. Upon entering the coexistence regime ($P \sim 2$ GPa; or-

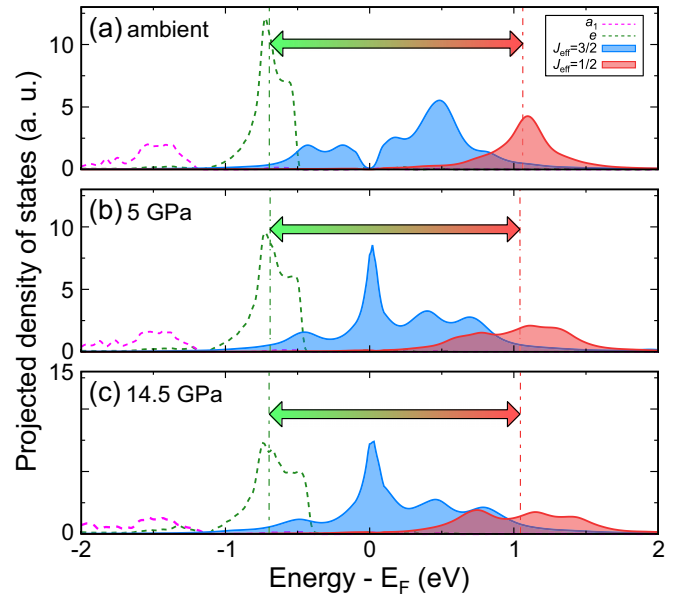


FIG. 4. (a)–(c) Calculated spectral functions at (a) $P = 0$, (b) 5, and (c) 14.5 GPa. The filled blue and red solid lines represent the molecular $J_{\text{eff}} = 3/2$ and $J_{\text{eff}} = 1/2$ states, respectively. The dashed magenta and green lines present the a_1 and e states, respectively. The arrows connect the center-of-mass positions of the $J_{\text{eff}} = 1/2$ and e states.

angle symbols), the peak becomes broadened with its intensity reduced. Up to 6 GPa, the peak width and energy are insensitive to the pressure. In the metallic phase ($P = 8$ and 10.4 GPa; gray and black symbols), the peak width is further broadened. A more itinerant $J_{\text{eff}} = 3/2$ state may contribute to the peak broadening in the high-pressure metallic phase by affecting the local coherent RIXS process. Consistent with the ambient pressure RIXS study, the insulating phase spectrum ($P = 0.9$ GPa; red symbols) shows that the 1.3-eV orbital excitation seen at the L_3 edge is totally suppressed at the L_2 edge due to the destructive quantum interference of the J_{eff} state. Importantly, the spectral intensity profile in the 1.3-eV excitation region is insensitive to the applied higher pressure up to 10.4 GPa, confirming that the J_{eff} state persists in the high-pressure metallic phase.

Arguably, this is the first verification of a metallic phase hosting $J_{\text{eff}} = 3/2$ moments. In the most-studied case of a metallic phase derived from a magnetic Mott insulator (e.g., cuprates), the magnetic order is quickly destroyed by doping. Recalling that the doping of a Mott insulator with $S = 1/2$ moments can lead to different intriguing phases such as the pseudogap phase and the strange metal phase, or superconductivity, our finding of a metallic $J_{\text{eff}} = 3/2$ phase deserves further investigations regarding its nature and relation to superconductivity, which are discussed further below.

Metallic $J_{\text{eff}} = 3/2$ states: DFT + DMFT calculations. In order to further elucidate the characteristics of this metallic phase, we performed many-body electronic structure calculations. The DFT + DMFT spectral functions are presented in Fig. 4. At ambient pressure [Fig. 4(a)], the Mott gap is clearly observed and the upper and lower Hubbard bands are of $J_{\text{eff}} = 3/2$ character. The gap size of 0.4–0.6 eV is in good

agreement with optical conductivity data [17]. At $P \geq 5$ GPa [Figs. 4(b) and 4(c)], the gap is closed and the system becomes metallic, with a characteristic quasiparticle peak forming at E_F . It should be noted that this correlated metallic feature of the spectral function cannot be captured by the static approximation. See Supplemental Material for more details [25].

An important observation is that the center-of-mass position of the higher-lying $J_{\text{eff}} = 1/2$ states does not move but remains basically unchanged, even though the spectral weight of the $J_{\text{eff}} = 1/2$ states is significantly redistributed by varying pressure. The arrows in Fig. 4 connect the center-of-mass positions of the e (dashed green lines) and $J_{\text{eff}} = 1/2$ (red solid lines) states, and their length is almost independent of the pressure.

This is particularly important because the $J_{\text{eff}} = 1/2 \rightarrow e$ transition is mainly responsible for the L_3 peak at +1.3 eV observed in our RIXS measurement [see Fig. 3(a)] [21]. Therefore, our DMFT calculation (including SOC) strongly supports our interpretation of the RIXS spectra; namely, the 1.3-eV peak should persist even for the reshaped spectral functions in the metallic phase [28]. An additional supporting analysis can be found in Ref. [25].

Another noticeable feature is that the low-energy states (forming the ‘‘coherent peak’’) in the metallic phase are still of the $J_{\text{eff}} = 3/2$ character [see Figs. 4(b) and 4(c)]. This may have important implications for superconductivity. Recalling the cuprate phase diagram, for example, the Mott-insulating state with antiferromagnetic spin order is destroyed by doping and followed by a pseudogap phase before superconductivity appears at low temperature. At higher temperatures, the pseudogap state is followed by the so-called strange metal, whose characteristics are clearly distinct from a Fermi liquid. In studies of the two-dimensional Hubbard model, it has recently been shown that these non-Fermi liquid phases host long-lived composite spin-1 moments [29,30]. In this regard, identifying the $J_{\text{eff}} = 3/2$ nature of the metallic phase of GaTa_4Se_8 may be relevant for understanding the superconductivity observed at higher pressures.

To gain further insights into the character of this distinct metallic phase, we perform a self-energy analysis. The renormalization factor Z , defined as $\lim_{\omega \rightarrow 0} [1 - \frac{\partial}{\partial \omega} \text{Re}\Sigma(\omega)]^{-1}$, shows that this pressure-induced phase exhibits sizable electronic correlations, which is reminiscent of the pseudogap or strange metal region of cuprates. Figure 5(a) shows that $Z_{J_{\text{eff}}=3/2}$ (blue circles) is well below 1.0 while it gradually increases as a function of pressure. This is in contrast to the result for the $J_{\text{eff}} = 1/2$ bands (red triangles) whose Z values remain close to unity in a wide pressure range.

For cuprates, the relation between the pseudogap phase and superconductivity has long been a central topic of research [2–4,6,30,31]. Also, recent theoretical studies on half Heusler alloys suggest possible superconductivity arising from a $J = 3/2$ band structure [32–36]. Here it is presumed that the observed superconductivity at higher pressure is unconventional since it emerges out of a distinct correlated metallic phase with $J_{\text{eff}} = 3/2$ in proximity to a Mott insulator.

Doping and spin-freezing superconductivity. Finally, we explore and suggest another intriguing possibility in this material. Recent multiband DMFT calculations have shown that unconventional superconductivity can arise from a so-called

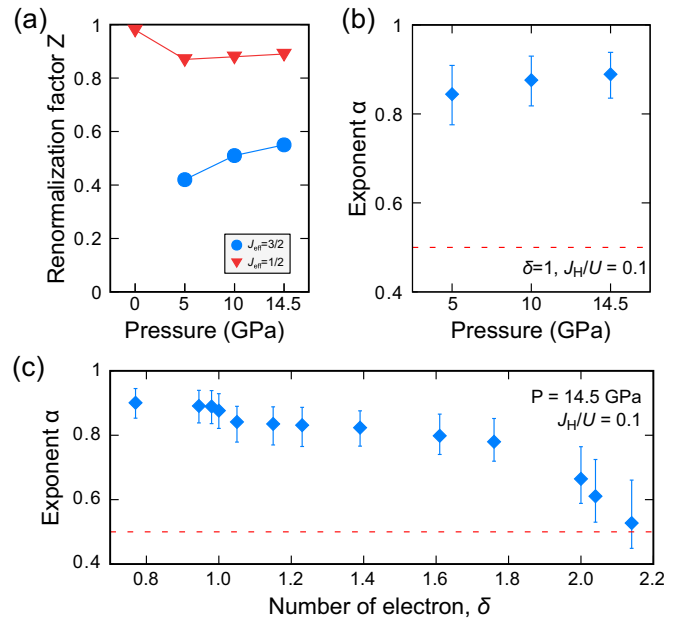


FIG. 5. (a) Calculated renormalization factor Z as a function of pressure. Blue circles (red triangles) show the Z values of the $J_{\text{eff}} = 3/2$ ($J_{\text{eff}} = 1/2$) bands. [(b),(c)] The calculated exponent α as a function of (b) pressure and (c) electron number. The horizontal red dashed lines show $\alpha = 0.5$, namely, the exponent value typically associated with a spin-freezing crossover [37]. The density of electrons $\delta = 1$ corresponds to pristine GaTa_4Se_8 . For the exponent fitting, $J_H/U = 0.1$ is used with $U = 0.8$ eV.

spin-freezing crossover [22,29,37–39], although this mechanism still requires experimental confirmation. In order to check this scenario in the case of GaTa_4Se_8 , we perform a self-energy analysis. Following Ref. [37], $-\text{Im}\Sigma(i\omega_n)$ is fitted in the low-energy region with the function $\Gamma + C(\omega_n)^\alpha$, where Γ , C , and α are constants, and ω_n denotes Matsubara frequencies. A Fermi liquid is characterized by $\text{Im}\Sigma(i\omega_n) \sim \omega_n$, namely, $\Gamma \approx 0$ and $\alpha \approx 1.0$ [40–42]. In the moment-freezing regime, on the other hand, the self-energy behavior clearly deviates from this linear dependence [40,41], with $\alpha < 1$.

The calculated α is presented as a function of pressure in Fig. 5(b) with $J_H/U = 0.1$ where we considered the range of $0.1 \lesssim \omega_n/D \lesssim 0.3$ (D is the half bandwidth) for the fitting. The error bars reflect the deviations caused by varying the fitting range [25]. In the metallic regime of $P \geq 5$ GPa, α increases as a function of pressure, which is reasonable in the sense that the system becomes more metallic or closer to a Fermi liquid. Note that α is well above the value $\alpha = 1/2$ typically associated with the spin-freezing crossover, which may indicate that the known pressure-induced superconductivity is not primarily driven by local moment fluctuations. In fact, in this $\delta = 1$ system with one electron per t_2 molecular orbital, the role of the Hund’s interaction J_H likely becomes less pronounced [40,42], although a J -freezing crossover has been reported in model calculations [38] with SOC.

On the other hand, we clearly find that introducing extra charges induces a moment-freezing crossover in GaTa_4Se_8 . Figure 5(c) shows the calculated exponent α as a function of δ (the electron number per t_2 molecular orbital). While Γ

remains quite small, α is gradually decreased as δ increases. In particular, at around $\delta \approx 1.8$ – 2.0 , a substantial drop is observed, indicative of a spin-freezing crossover [37]. This result is also consistent with the previous model study on a Bethe lattice [38]. Thus, an unconventional type of superconductivity, possibly distinct from the pressure-induced superconductivity at zero doping, can be expected to occur under electron doping.

In order to introduce extra electrons into GaTa_4X_8 , the chemical substitution of Ge for Ga can be considered and has been already reported for $(\text{Ga/Ge})\text{V}_4\text{S}_8$ [43]. Doping alkali- or alkaline-earth metals is another possible way to achieve a spin-freezing crossover. As a “deficient” spinel structure (i.e., AB_2X_4 spinel with half-deficient A sites), lacunar spinels can likely host additional alkali- or alkaline-earth metals. While a spin-freezing crossover has been previously suggested for multiband transition-metal perovskite oxides [40], it is awaiting experimental confirmation. Here we note that this prediction is based on the idealized model density of states (DOS) of the Bethe lattice. While the spin-freezing crossover appears in between two extreme limits of spin states, this idealized DOS shape can easily be broken up in a real material. Then the system is driven to more stable ordered phases such as antiferromagnetic, ferromagnetic, and/or orbital ordered phases, rather than the less stable superconducting phase. This may be the reason why in many multiband perovskite oxides no superconductivity has been identified. In this regard, GaTa_4X_8 can be an interesting playground because its DOS shape is better retained due to its molecular nature. Namely, even under pressure, the lattice degree of freedom is less active and the electronic degeneracy is well maintained. In fact, the main change of the lattice structure as a function of pressure is the reduction of the

intercluster distance, while the molecular units are largely unchanged [16]. Thus GaTa_4Se_8 can be an ideal platform to explore this type of unconventional superconductivity.

Summary. We demonstrated that the metallic phase of GaTa_4Se_8 carries $J_{\text{eff}} = 3/2$ moments and exhibits sizable correlations. Our RIXS spectra clearly show that the characteristic orbital excitation features are well maintained under pressure, which is consistent with the results of our DFT + DMFT calculations. The pressure-induced phase can therefore be regarded as a distinct type of correlated metallic phase. Simultaneously, this conclusion suggests that the superconductivity appearing at higher pressure is likely unconventional. Furthermore, our self-energy analysis indicates that an unconventional type of superconductivity may emerge from a J -freezing crossover under electron doping. Our results highlight a distinct material phase, which provides an exciting playground for exploring unconventional types of superconducting instabilities.

Acknowledgments. The use of the Advanced Photon Source at the Argonne National Laboratory was supported by the U.S. Department of Energy (DOE) under Contract No. DE-AC02-06CH11357. M.Y.J., J.-H.S., and M.J.H. were supported by the Basic Science Research Program (Grant No. 2018R1A2B2005204) and the Creative Materials Discovery Program through the National Research Foundation (NRF) of Korea (Grant No. 2018M3D1A1058754) funded by the Ministry of Science and ICT (MSIT) of Korea, and by the KAIST Grand Challenge 30 Project (KC30) in 2019 funded by the MSIT of Korea and KAIST. H.J.L. and A.G. were supported by the Institute for Basic Science under Grant No. IBS-R024-D1.

M.Y.J. and S.H.C. contributed equally to this work.

-
- [1] E. Fradkin, S. A. Kivelson, and J. M. Tranquada, *Rev. Mod. Phys.* **87**, 457 (2015).
 - [2] M. R. Norman, D. Pines, and C. Kallin, *Adv. Phys.* **54**, 715 (2005).
 - [3] P. A. Lee, N. Nagaosa, and X.-G. Wen, *Rev. Mod. Phys.* **78**, 17 (2006).
 - [4] B. Keimer and J. E. Moore, *Nat. Phys.* **13**, 1045 (2017).
 - [5] D. N. Basov, R. D. Averitt, D. van der Marel, M. Dressel, and K. Haule, *Rev. Mod. Phys.* **83**, 471 (2011).
 - [6] D. J. Scalapino, *Rev. Mod. Phys.* **84**, 1383 (2012).
 - [7] A. Kapitulnik, S. A. Kivelson, and B. Spivak, *Rev. Mod. Phys.* **91**, 011002 (2019).
 - [8] I. Kézsmárki, S. Bordács, P. Milde, E. Neuber, L. M. Eng, J. S. White, H. M. R. onnow, C. D. Dewhurst, M. Mochizuki, K. Yanai, H. Nakamura, D. Ehlers, V. Tsurkan, and A. Loidl, *Nat. Mater.* **14**, 1116 (2015).
 - [9] E. Ruff, S. Widmann, P. Lunkenheimer, V. Tsurkan, S. Bordács, I. Kézsmárki, and A. Loidl, *Sci. Adv.* **1**, e1500916 (2015).
 - [10] Y. Fujima, N. Abe, Y. Tokunaga, and T. Arima, *Phys. Rev. B* **95**, 180410(R) (2017).
 - [11] E. Ruff, A. Butykai, K. Geirhos, S. Widmann, V. Tsurkan, E. Stefanet, I. Kézsmárki, A. Loidl, and P. Lunkenheimer, *Phys. Rev. B* **96**, 165119 (2017).
 - [12] K. Geirhos, S. Krohns, H. Nakamura, T. Waki, Y. Tabata, I. Kézsmárki, and P. Lunkenheimer, *Phys. Rev. B* **98**, 224306 (2018).
 - [13] V. Guiot, E. Janod, B. Corraze, and L. Cario, *Chem. Mater.* **23**, 2611 (2011).
 - [14] V. Dubost, T. Cren, C. Vaju, L. Cario, B. Corraze, E. Janod, F. Debontridder, and D. Roditchev, *Nano Lett.* **13**, 3648 (2013).
 - [15] M. M. Abd-Elmeguid, B. Ni, D. I. Khomskii, R. Pocha, D. Johrendt, X. Wang, and K. Syassen, *Phys. Rev. Lett.* **93**, 126403 (2004).
 - [16] R. Pocha, D. Johrendt, B. Ni, and M. M. Abd-Elmeguid, *J. Am. Chem. Soc.* **127**, 8732 (2005).
 - [17] V. Ta Phuoc, C. Vaju, B. Corraze, R. Sopracase, A. Perucchi, C. Marini, P. Postorino, M. Chligui, S. Lupi, E. Janod, and L. Cario, *Phys. Rev. Lett.* **110**, 037401 (2013).
 - [18] A. Camjayi, C. Acha, R. Weht, M. G. Rodríguez, B. Corraze, E. Janod, L. Cario, and M. Rozenberg, *Phys. Rev. Lett.* **113**, 086404 (2014).
 - [19] B. J. Kim, H. Jin, S. J. Moon, J.-Y. Kim, B.-G. Park, C. S. Leem, J. Yu, T. W. Noh, C. Kim, S.-J. Oh, J.-H. Park, V. Durairaj, G. Cao, and E. Rotenberg, *Phys. Rev. Lett.* **101**, 076402 (2008).
 - [20] H.-S. Kim, J. Im, M. J. Han, and H. Jin, *Nat. Commun.* **5**, 3988 (2014).

- [21] M. Y. Jeong, S. H. Chang, B. H. Kim, J.-H. Sim, A. Said, D. Casa, T. Gog, E. Janod, L. Cario, S. Yunoki, M. J. Han, and J. Kim, *Nat. Commun.* **8**, 782 (2017).
- [22] S. Hoshino and P. Werner, *Phys. Rev. Lett.* **115**, 247001 (2015).
- [23] R. Pocha, D. Johrendt, and R. Pöttgen, *Chem. Mater.* **12**, 2882 (2000).
- [24] A. Camjayi, R. Weht, and M. J. Rozenberg, *Europhys. Lett.* **100**, 57004 (2012).
- [25] See Supplemental Material at <http://link.aps.org/supplemental/10.1103/PhysRevB.103.L081112> for computational details, experimental details, and complementary data, which include Refs. [44–62].
- [26] M. Casula, P. Werner, L. Vaugier, F. Aryasetiawan, T. Miyake, A. J. Millis, and S. Biermann, *Phys. Rev. Lett.* **109**, 126408 (2012).
- [27] J. Kim, *High Pressure Res.* **36**, 391 (2016).
- [28] This weight transfer might be responsible for the reduction of the L_3 RIXS peak height as a function of pressure [see Fig. 3(b)], which needs further clarification.
- [29] P. Werner, S. Hoshino, and H. Shinaoka, *Phys. Rev. B* **94**, 245134 (2016).
- [30] P. Werner, X. Chen, and E. Gull, *Phys. Rev. Research* **2**, 023037 (2020).
- [31] E. Gull, O. Parcollet, and A. J. Millis, *Phys. Rev. Lett.* **110**, 216405 (2013).
- [32] P. M. Brydon, L. Wang, M. Weinert, and D. F. Agterberg, *Phys. Rev. Lett.* **116**, 177001 (2016).
- [33] C. Timm, A. P. Schnyder, D. F. Agterberg, and P. M. R. Brydon, *Phys. Rev. B* **96**, 094526 (2017).
- [34] H. Kim, K. Wang, Y. Nakajima, R. Hu, S. Ziemak, P. Syers, L. Wang, H. Hodovanets, J. D. Denlinger, P. M. R. Brydon, D. F. Agterberg, M. A. Tanatar, R. Prozorov, and J. Paglione, *Sci. Adv.* **4**, eaao4513 (2018).
- [35] J. W. F. Venderbos, L. Savary, J. Ruhman, P. A. Lee, and L. Fu, *Phys. Rev. X* **8**, 011029 (2018).
- [36] G. B. Sim, A. Mishra, M. J. Park, Y. B. Kim, G. Y. Cho, and S. B. Lee, *Phys. Rev. B* **100**, 064509 (2019).
- [37] P. Werner, E. Gull, M. Troyer, and A. J. Millis, *Phys. Rev. Lett.* **101**, 166405 (2008).
- [38] A. J. Kim, H. O. Jeschke, P. Werner, and R. Valentí, *Phys. Rev. Lett.* **118**, 086401 (2017).
- [39] P. Werner and S. Hoshino, *Phys. Rev. B* **101**, 041104(R) (2020).
- [40] A. Georges, L. d. Medici, and J. Mravlje, *Annu. Rev. Condens. Matter Phys.* **4**, 137 (2013).
- [41] A. Kowalski, A. Hausoel, M. Wallerberger, P. Gunacker, and G. Sangiovanni, *Phys. Rev. B* **99**, 155112 (2019).
- [42] K. Stadler, G. Kotliar, A. Weichselbaum, and J. von Delft, *Ann. Phys.* **405**, 365 (2019).
- [43] E. Janod, E. Dorolti, B. Corraze, V. Guiot, S. Salmon, V. Pop, F. Christien, and L. Cario, *Chem. Mater.* **27**, 4398 (2015).
- [44] T. Ozaki, *Phys. Rev. B* **67**, 155108 (2003).
- [45] I. Leonov, A. I. Poteryaev, V. I. Anisimov, and D. Vollhardt, *Phys. Rev. Lett.* **106**, 106405 (2011).
- [46] K. Haule and T. Birol, *Phys. Rev. Lett.* **115**, 256402 (2015).
- [47] I. Leonov, S. L. Skornyakov, V. I. Anisimov, and D. Vollhardt, *Phys. Rev. Lett.* **115**, 106402 (2015).
- [48] S. L. Skornyakov, V. I. Anisimov, D. Vollhardt, and I. Leonov, *Phys. Rev. B* **96**, 035137 (2017).
- [49] N. Marzari and D. Vanderbilt, *Phys. Rev. B* **56**, 12847 (1997).
- [50] I. Souza, N. Marzari, and D. Vanderbilt, *Phys. Rev. B* **65**, 035109 (2001).
- [51] F. Aryasetiawan, K. Karlsson, O. Jepsen, and U. Schönberger, *Phys. Rev. B* **74**, 125106 (2006).
- [52] E. Şaşıoğlu, C. Friedrich, and S. Blügel, *Phys. Rev. B* **83**, 121101(R) (2011).
- [53] D. Sénéchal, *Phys. Rev. B* **81**, 235125 (2010).
- [54] A. Go and A. J. Millis, *Phys. Rev. Lett.* **114**, 016402 (2015).
- [55] A. Go and A. J. Millis, *Phys. Rev. B* **96**, 085139 (2017).
- [56] E. Fertitta and G. H. Booth, *Phys. Rev. B* **98**, 235132 (2018).
- [57] N.-O. Linden, M. Zingl, C. Hubig, O. Parcollet, and U. Schollwöck, *Phys. Rev. B* **101**, 041101(R) (2020).
- [58] Y. Shvyd'ko, J. Hill, C. Burns, D. Coburn, B. Brajuskovic, D. Casa, K. Goetze, T. Gog, R. Khachatryan, J.-H. Kim, C. Koditwakkhu, M. Ramanathan, T. Roberts, A. Said, H. Sinn, D. Shu, S. Stoupin, M. Upton, M. Wiczorek, and H. Yavas, *J. Electron. Spectrosc. Relat. Phenom.* **188**, 140 (2013).
- [59] M. Rossi, C. Henriquet, J. Jacobs, C. Donnerer, S. Boseggia, A. Al-Zein, R. Fumagalli, Y. Yao, J. G. Vale, E. C. Hunter, R. S. Perry, I. Kantor, G. Garbarino, W. Crichton, G. Monaco, D. F. McMorrow, M. Krisch, and M. M. Sala, *J. Synchrotron Radiat.* **26**, 1725 (2019).
- [60] G. Kotliar, S. Y. Savrasov, K. Haule, V. S. Oudovenko, O. Parcollet, and C. A. Marianetti, *Rev. Mod. Phys.* **78**, 865 (2006).
- [61] H.-S. Kim, K. Haule, and D. Vanderbilt, *Phys. Rev. B* **102**, 081105(R) (2020).
- [62] Z. P. Yin, K. Haule, and G. Kotliar, *Phys. Rev. B* **86**, 195141 (2012).